Engineering and Applied Science Research

Numerical investigation of nanofluid flow and heat transfer over a backward-facing step

Pedram Pournaderi* and Milad Aram

Department of Mechanical Engineering, Faculty of Engineering, Yasouj University, Yasouj, Iran

Abstract

In this research, the forced convection heat transfer of a nanofluid in a channel with a backward- facing step is studied by adopting the finite volume technique. The effect of nanoparticles is considered by employing the single-phase model. The influence of various parameters is considered on both pressure drop and Nusselt number. The local Nusselt number increases after the step as a result of the recirculation of flow. However, the average Nusselt number decreases as the step height increases. Increasing the step height also decreases the pressure drop. The pressure drop and Nusselt number both increases with nanoparticle's concentration and Reynolds number. The pressure drop enhancement is very intense for the volume fraction of 0.04. Increasing nanoparticle diameter decreases both the pressure drop and Nusselt number. Six types of nanoparticles (TiO$_2$, Fe$_3$O$_4$, CuO, Al$_2$O$_3$, ZnO, SiO$_2$) were compared. The maximum average Nusselt number was related to Water-TiO$_2$ nanofluid. It was also concluded that the effect of the nanofluid type on the pressure drop is not considerable. The performance index decreases with the Reynolds number slightly. Also, for concentrations of 3% and 4%, the performance index reduces considerably.

Nomenclature

C	Specific heat capacity, (J/(kg.K))	$\vec{V}$	Velocity vector, (m/s)
d	Equivalent diameter of a molecule or a nanoparticle, (m)	x, y	Cartesian coordinates, (m)
f	Average friction factor		
H	Channel height at outlet, (m)	*Greek characters*	
h	Local heat transfer coefficient, (W/(m^2.K))	ϕ	Volume fraction
k	Thermal conductivity, (W/(m.K))	μ	Dynamic viscosity, ((N.s)/m^2)
K	Boltzmann constant, (J/K)	ρ	Density, (kg/m^3)
M	Base fluid molecular weight, (gr/mole)	τ	Viscose stress tensor, (N/m^2)
N	Avogadro's number		
Nu	Nusselt number	*Subscripts*	
PI	Performance index	ave	Average value
p	Pressure, (N/m^2)	f	Base fluid
q	Heat flux, (W/m^2)	∞	Values at inlet
Re	Reynolds number	nf	Nanofluid
s	Step height, (m)	np	Nanoparticle
T	Temperature, (K)	p	Constant pressure or particle
u, v	x, y velocity components, (m/s)	0	Reference value

1. Introduction

There are different methods for enhancing the thermal efficiency of heat exchanging systems. Using expansion or contraction in the channel flow is a common method for enhancing the heat transfer rate. There are many studies in this regard. Addad et al. [1] simulated the turbulent flow in a channel with a forward-facing step by employing the Large Eddy Simulation (LES) and reported the ratio of the reattachment offset and separation length to the step height. Abu-Mulaweh [2] studied the turbulent convective flow over an inclined forward-facing step numerically. He considered the influence of expansion ratio, Reynolds and Prandtl numbers on the heat transfer rate. Chen et al. [3] studied the airflow in a one-sided contracting channel both experimentally and numerically. They reported that the

Nusselt number is independent of the Reynolds number and the maximum local Nusselt number occurs near the reattachment point. Abu-Nada [4] studied the entropy generation in a one-sided contracting channel flow numerically. He reported that enhancement of the Reynolds number enhances the total entropy generation. Lima et al. [5] studied the laminar flow over a backward-facing step in a channel by using both finite volume and finite element methods. They concluded that the difference between the numerical and experimental results enhances when the recirculation on the top wall and the second recirculation on the bottom wall occurs. Sherry et al. [6] conducted an experiment to study the flow in a channel withr a forward-facing step and describe the mechanisms that play an important role on the reattachment length. Bao and Lin [7] simulated the transition regime in a microscale backward-facing step. They found out that the mass flow rate increases as the pressure ratio increases and this relation is nonlinear in spite of the traditional flow. Kumar and Dhiman [8] simulated the flow over a backward-facing step in a channel containing a stationary cylinder. They reported that if the cylinder is located in an appropriate position, the heat transfer rate increases considerably. Selimefendigil and Oztop [9] studied the rotating cylinder influence on the flow of a ferrofluid over a backward-facing step in the presence of a magnetic field. They concluded that the magnetic field strength and the cylinder rotation angle can be used to control the size and length of the recirculation regions. Togun et al. [10] simulated the fluid flow over a backward-facing step in the presence of an obstacle. They found the obstacle increases the heat transfer rate. This increase is due to the recirculation zone which is created after the obstacle. Niemann and Frohlich [11] simulated the turbulent flow over a backward-facing step in a vertical channel. They studied the effect of the buoyancy term. They reported that in the presence of the buoyancy forces the flow field considerably changes, recirculation is substantially reduced and the heat transfer rate increases. Xu et al. [12] simulated the flow over a backward-facing step in the three-dimensional case and studied the Reynolds number effect. They observed a peak value in the time-averaged reattachment length at Re=1000. After that, increasing the Reynolds number decreases the time averaged reattachment length. Juste and Fajardo [13] studied the laminar and early transitional flow over a backward-facing step in a narrow channel by employing the large eddy simulation. They found out in the early transitional regime, the influence of the lateral surfaces on the heat transfer is negative.

The use of nanofluids in heat exchanging equipment has been grown extensively in recent years. The reason is the higher conductivity of the nanofluids in comparison with the pure fluids. Al-aswadi et al. [14] investigated the forced convection flow of nanofluids in a channel with a backward-facing step numerically. They found that increasing the Reynolds number causes the reattachment point to move downstream far from the step. In addition, the wall shear stress increases by increasing the Reynolds number. Kherbeet et al. [15] studied the heat transfer of nanofluid over a microscale backward-facing step numerically. They observed that increasing the Reynolds number enhances the friction coefficient. In addition, the Nusselt number increases with the nanoparticle's concentration and Reynolds number. Selimefendigil and Oztop [16] simulated the pulsating nanofluid flow in a backward-facing step channel containing a cylinder. They reported that the heat transfer rate increases with the frequency of the oscillation, nanoparticle concentration and, Reynolds number. Kherbeet et al. [17]

investigated the laminar flow of nanofluid over a microscale backward-facing step both numerically and experimentally. They compared water-silica and water-alumina nanofluids and concluded that the Nusselt number for the water-silica nanofluid flow is higher. In addition, the water-alumina has a higher friction factor in comparison with the water-siltude mixture. Selimefendigil and Oztop [18] simulated the laminar nanofluid flow over a backward-facing step with a corrugated bottom surface by using the finite element method. They evaluated the influence of locating different shaped obstacles in the channel and concluded that the diamond-shaped obstacle shows better heat transfer characteristics in comparison with the circular and square-shaped obstacles. Selimefendigil and Oztop [19] investigated numerically the pulsating nanofluid flow in a one-sided expanding channel with a corrugated bottom wall. They found that increasing the Reynolds number, height and length of the corrugation wave increases the Nusselt number. In addition, the enhancement of the pulsation amplitude enhances the heat transfer rate. Bouazizi [20] simulated the copper-water nanofluid flow in a backward- facing step channel with a heated square obstacle located behind the first primary recirculation region. Based on the results the heated square obstacle enhances the heat transfer rate. The heat transfer enhancement is more considerable at higher Richardson number and nanoparticle concentration. Ekiciler et al. [21] studied the alumina-water nanofluid flow in a one-sided expanding channel numerically. The nanoparticle diameter, step height, and channel height were considered constant. They reported that enhancement of the nanoparticle concentration and Reynolds number increases the Nusselt number. Mohammed et al. [22] conducted a numerical study on the mixed convection heat transfer of nanofluid over a backward-facing step in the presence of an obstacle. They performed simulations for four types of obstacle shapes (circular, back-facing triangular, front-facing triangular and, trapezoidal). It was concluded that the front-facing triangular and the trapezoidal obstacles have the highest and lowest value of average Nusselt number, respectively.

According to the literature, many investigations have been conducted on the nanofluid flow in a channel with a backward-facing step. In the previous studies mainly the effects of the Reynolds number and nanoparticle concentration on the heat transfer have been reported. To the best of the current authors' knowledge, there is no comprehensive investigation on this problem which considers the effect of different quantities such as Reynolds number, step height, nanoparticle's concentration, nanoparticle's diameter and nanofluid type on both pressure drop and heat transfer. In the current research, the nanofluid flow in a channel with a backward-facing step is simulated and the influence of the mentioned parameters on both heat transfer and pressure drop is investigated.

2. Governing equations

2.1. Flow and energy equations

The governing equations are the continuity and momentum equations in incompressible case:

$$\nabla \cdot \vec{V} = 0 \tag{1}$$

$$(\vec{V} \cdot \nabla)\vec{V} = -\frac{1}{\rho}\nabla p - \frac{1}{\rho}\nabla \cdot \tau \tag{2}$$

where, $\vec{V} = (u, v)$, ρ, p, and, τ represent velocity field, density, pressure and, viscous stress tensor, respectively. τ is stated as follows:

$$\tau = \mu \begin{pmatrix} \nabla u \\ \nabla v \end{pmatrix} + \mu \begin{pmatrix} \nabla u \\ \nabla v \end{pmatrix}^T \tag{3}$$

where μ stands for dynamic viscosity.

To obtain the heat transfer, it is necessary to compute the temperature distribution. The temperature equation is expressed as follows:

$$(\vec{V} \cdot \nabla)T = \frac{\nabla \cdot (k\nabla T)}{\rho C_p} \tag{4}$$

where T, k and C_p represent temperature, thermal conductivity and specific heat capacity at constant pressure, respectively.

2.2. Thermo-physical properties of nanofluid

In this investigation, the single-phase model is used to consider the effect of nanoparticles. A nanofluid suspension is a two-phase fluid. However, under specific assumptions, nanofluid can be supposed as a homogenous liquid. Since nanoparticles are extremely fine, it is supposed that they easily disperse in the bulk fluid and both the bulk fluid and nanoparticles are in thermal equilibrium. Also, there is no slip between bulk fluid and nanoparticles. Under these assumptions, nanofluid is considered as a single-phase fluid with constant properties. These constant values are determined based on nanoparticles concentration, nanoparticles properties, and base fluid properties. In this study, the following equations are employed to compute the nanofluid properties. In these equations, indices f and np refer to base fluid and nanoparticle, respectively.
The nanofluid density is computed as [10]:

$$\rho_{nf} = (1 - \phi)\rho_f + \phi\rho_{np} \tag{5}$$

where ϕ represents nanoparticles volume fraction.

The following equation is employed to calculate the effective viscosity of nanofluid [10]:

$$\mu_{nf} = \mu_f \times \frac{1}{(1 - 34.87(d_p/d_f)^{-0.3} \times \phi^{1.03})} \tag{6}$$

$$d_f = \left(\frac{6M}{N \pi \rho_{f\,0}} \right)^{1/3} \tag{7}$$

where d_f and d_p are the equivalent diameter of a molecule of the base fluid and the nanoparticles average diameter, respectively. $\rho_{f\,0}$ is the density of nanofluid at 293K. M and N represent the base fluid molecular weight and Avogadro's number (6.0221409e+23mol^{-1}), respectively.

The nanofluid heat capacity is obtained by the following relation [10]:

$$(\rho C_p)_{nf} = (1 - \phi)(\rho C_p)_f + \phi(\rho C_p)_{np} \tag{8}$$

The thermal conductivity of nanofluid is computed by employing the following equation [10]:

$$k_{nf} = k_{static} + k_{Brownian} \tag{9}$$

where,

$$k_{static} = k_f \left[\frac{(k_{np} + 2k_f) - 2\phi(k_f - k_{np})}{(k_{np} + 2k_f) + \phi(k_f + k_{np})} \right] \tag{10}$$

$$k_{Brownian} = 5 \times 10^4 \beta \phi \rho_f C_{p,f} \sqrt{\frac{KT}{2\rho_{np}d_p}} f(T, \phi) \tag{11}$$

In equation (11), the Boltzmann constant, K=1.3809*10^{-23} J/K. β and $f(T, \phi)$ are expressed as:

$$\beta = 8.4407(100\phi)^{-1.07304} \tag{12}$$

$$f(T, \phi) = (2.08217 \times 10^{-2}\phi + 3.917 \times 10^{-3})$$
$$\left(\frac{T}{T_0} \right) + (-3.0669 \times 10^{-2}\phi - 3.91123 \times 10^{-3}) \tag{13}$$

where the reference temperature, T_0, is 273 K.

3. Numerical methods

In this study, the finite volume technique is adopted for the discretization of the flow and energy equations on a structured (rectangular) mesh. The SIMPLE algorithm is used to solve the flow equations. The second-order upwind method is used for discretization of the convective terms. Also, the central approximation is employed to discretize the diffusion terms.

4. Results and discussion

In this research, the heat transfer of nanofluid flow over a two-dimensional backward-facing step is studied. Figure 1 describes the problem schematically. The dimensions of the channel in addition to boundary conditions have been presented in this figure. A heat flux of 2000 W/m^2 is applied on the downstream surface of the step. The other walls of the channel are considered to be insulated. The fluid temperature at the inlet is 300 K. The pressure and the gradient of other quantities at the outlet are considered to be zero. Table 1 represents the properties of water and nanoparticles which were used in the simulations.

4.1. Verification of the results

In this section, the water flow over a backward-facing step is simulated and the results are compared with the numerical results reported by Al-aswadi et al. [14] and Togun et al. [10]. The Reynolds number $\left(Re = \frac{\rho u_\infty H}{\mu} \right)$ is considered to be 175. A grid with a size of 128*60 is used for simulations. Figure 2 represents the velocity and temperature distribution in the channel. Note that only a part of the channel has been shown. The presence of the step leads to the flow separation and as a result, a recirculation zone is formed in the vicinity of the step. The circulation of the flow in this region effects on the temperature distribution. The highest temperature values are observed in this region. After the recirculation zone, the thermal boundary layer thickness increases gradually. Figure 3 shows the velocity profiles at two specific locations along the heated wall. At x/s=1.04 the velocity sign near the wall is negative which is due to the circulation of the flow near the step. After the reattachment
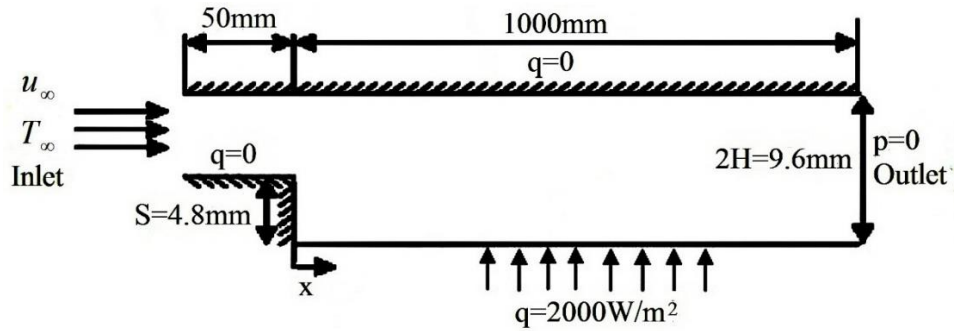
Figure 1 Schematic description of the problem
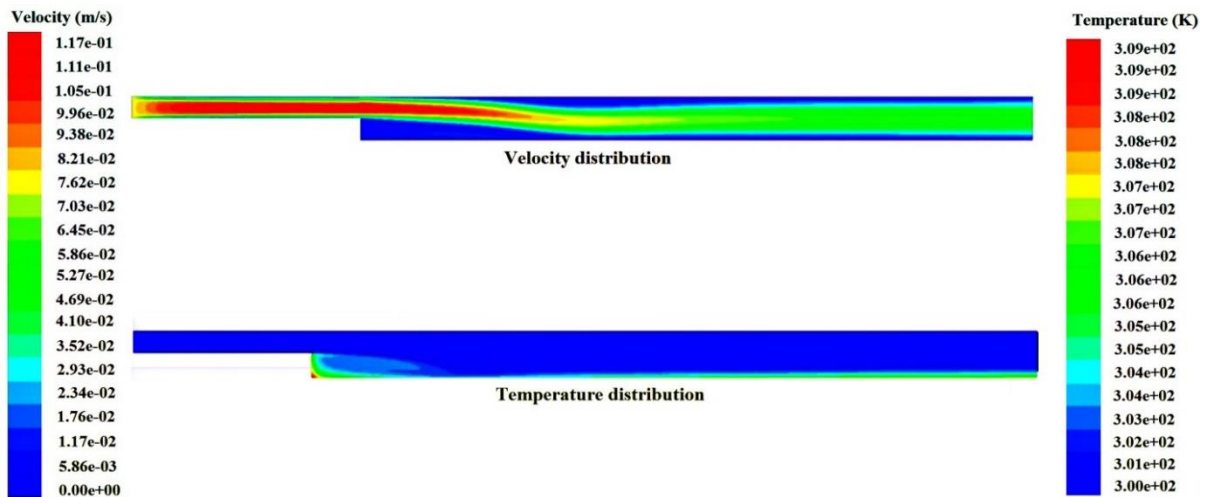
Figure 2 Velocity and temperature distribution
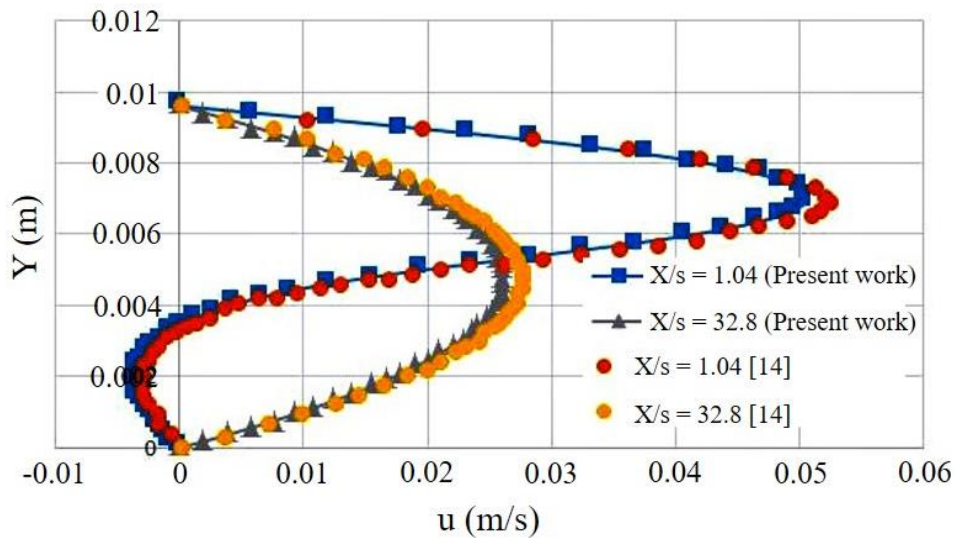
Figure 3 Comparison of the velocity profiles with the numerical results of Al-aswadi et al. [14] (Re=175)

Table 1 Thermo-physical properties of water and nanoparticles

	Cuo	*Al₂O₃*	*TiO₂*	*SiO₂*	*ZnO*	*Fe₃O₄*	*Water*
$\rho \ (kg/m^3)$	6500	996.5	5810	5610	2650	4260	3900
$C_p \ (J/kg \ K)$	533	4181	670	550	705	6890	780
$k \ (W/mK)$	17.65	0.613	30	1.2	2	11.7	36
$\mu \ (N.s/m^2)$	-	1E-03	-	-	-	-	-
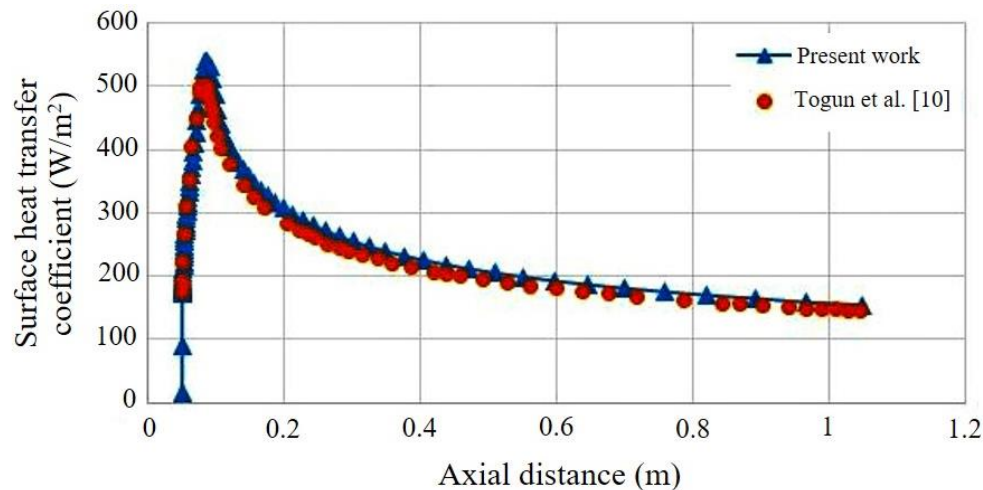
Figure 4 Comparison of the surface heat transfer coefficient with the numerical results of Togun et al. [10] (Re=175)
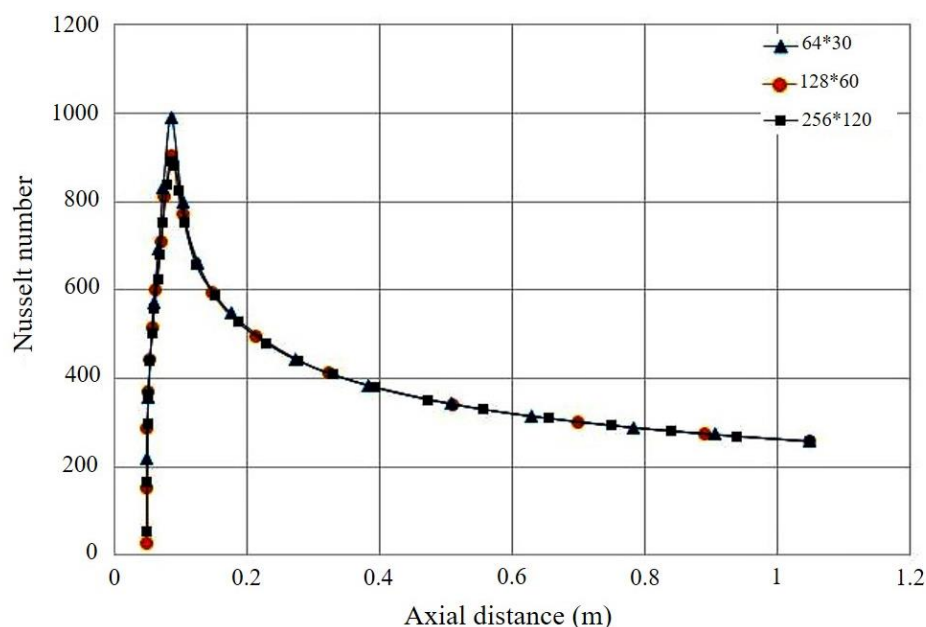
Figure 5 Variations of Nusselt number along the channel for different grids (Re=175)

point, the flow gradually becomes fully-developed. The fully-developed velocity profile can be observed in Figure 3 at x/s=32.8. In Figure 3 the simulation results have been compared with the numerical results of Al-aswadi et al. [14]. The agreement between the results is satisfactory. Figure 4 represents the surface heat transfer coefficient along the channel in comparison with the results of Togun et al. [10]. The agreement between the results is satisfactory. In the recirculation region, the heat transfer coefficient increases and reaches a maximum value near the reattachment point. Then, the heat transfer coefficient decreases due to the enhancement of the thermal boundary layer thickness.

Figure 5 shows the variations of the Nusselt number on the heated wall along the channel for three different mesh sizes. As it is observed, the difference between the results for the grids 128*60 and 256*120 is very small. This confirms that the selected grid (128*60) is appropriate for simulations.

For further verification of the work, the Cu/water nanofluid flow over a backward-facing step is simulated and compared with the numerical results of Togun et al. [23]. The

channel height at outlet is 2.5cm. Also, the step height, upstream length and downstream length are 1.25cm, 200cm and 150cm, respectively. A heat flux of 4000 W/m^2 is applied on the downstream surface of the step. The other walls are insulated. The Reynolds number and volume fraction of nanoparticles are considered to be 50 and 0.02, respectively. Figure 6 depicts the variations of the Nusselt number on the heated wall along the channel. According to this figure, the agreement between the results is satisfactory.

4.2. Reynolds number effect

In this section, the Reynolds number effect on the heat transfer and pressure drop along the channel are investigated for the CuO/Water nanofluid flow. The concentration of the nanofluid and nanoparticle's diameter are considered to be 0.02 and 20 nm, respectively. Figure 7 shows the variations of the Nusselt number on the heated wall along the channel for different Reynolds numbers. The Nusselt number increases as the Reynolds number increases. As it was stated
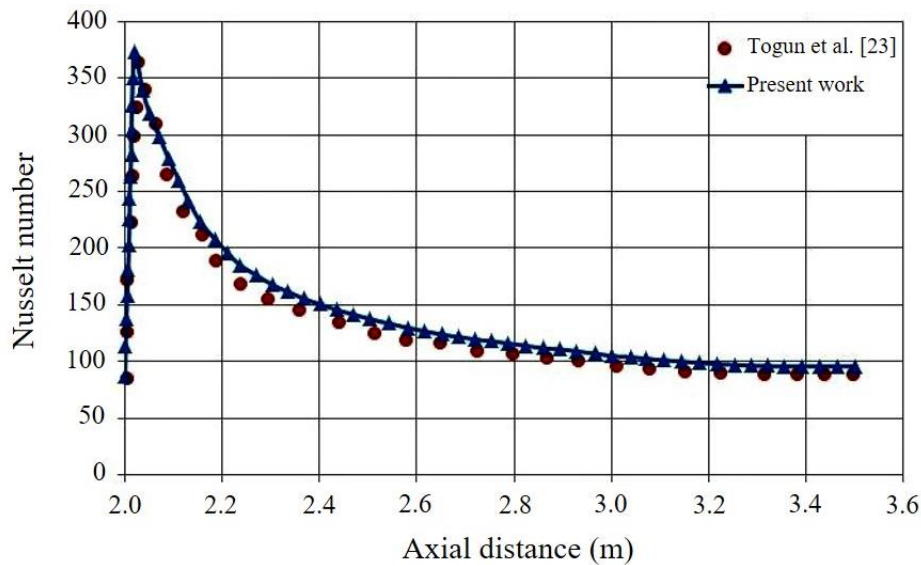
Figure 6 Comparison of the Nusselt number with the numerical results of Togun et al. [23] (Re=50)
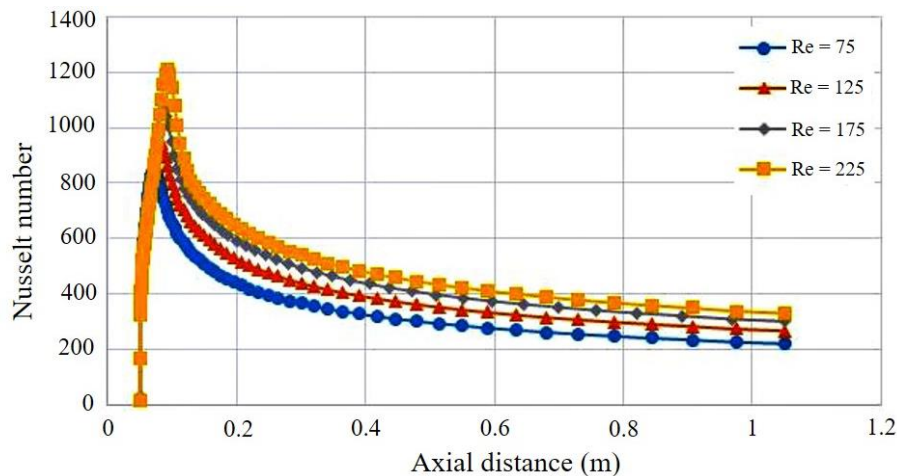
Figure 7 Variations of Nusselt number along the channel for different Reynolds numbers

before, the initial increase of the Nusselt number is originated from the recirculation of the flow after the step. The extent of the recirculation region increases by increasing the Reynolds number. Thus, the higher Reynolds number results in the higher Nusselt number. Figure 8 represents the variations of the pressure along the channel for different Reynolds numbers. The pressure decreases before the step due to the wall friction. After the expansion, it increases in the recirculation zone and then decreases until reaches the zero value at the exit. At higher Reynolds number, the recirculation region becomes wider and subsequently, the static pressure obtains a higher peak after the reattachment point. In this case, the hydrodynamic of the flow changes in a way that a higher pressure at the inlet is achieved. Therefore, it can be concluded the pressure drop along the channel increases with the Reynolds number.

Figure 9 depicts the average Nusselt number as a function of Reynolds number for different concentration of nanoparticles. It can be observed that the average Nusselt number increases as the Reynolds number increases. In this figure, the relationship between the average Nusselt number and the Reynolds number has been presented for each curve. Note that these relationships are only valid within the studied

range of Reynolds number. Figure 10 shows the average friction factor as a function of Reynolds number for different concentration of nanoparticles. According to this figure, the average friction factor decreases with the Reynolds number and increases with the concentration of nanoparticles. As the volume fraction increases to 4%, the average friction factor increases drastically. For further clarity, the friction factor values for the volume fraction of 4% have been presented in a separate frame. In this figure, the relationship between the average friction factor and the Reynolds number has been presented for each curve.

4.3. Step height effect

Now, the step height effect on the Nusselt number and pressure drop is considered. The Reynolds number, volume fraction of CuO and nanoparticle's diameter are 225, 0.02 and 10 nm, respectively. Figures 11 and 12 show the variations of Nusslet number and pressure versus axial distance for different step height values, respectively. When the step height enhances, a considerable enhancement in the Nusselt number is achieved in the recirculation region which is due to the stronger mixing of the flow after the step.
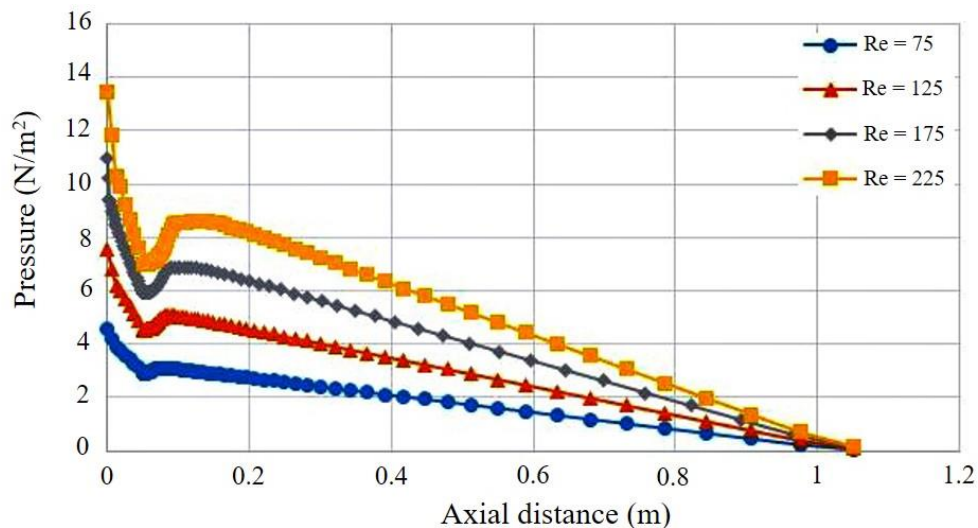
Figure 8 Variations of pressure along the channel for different Reynolds numbers
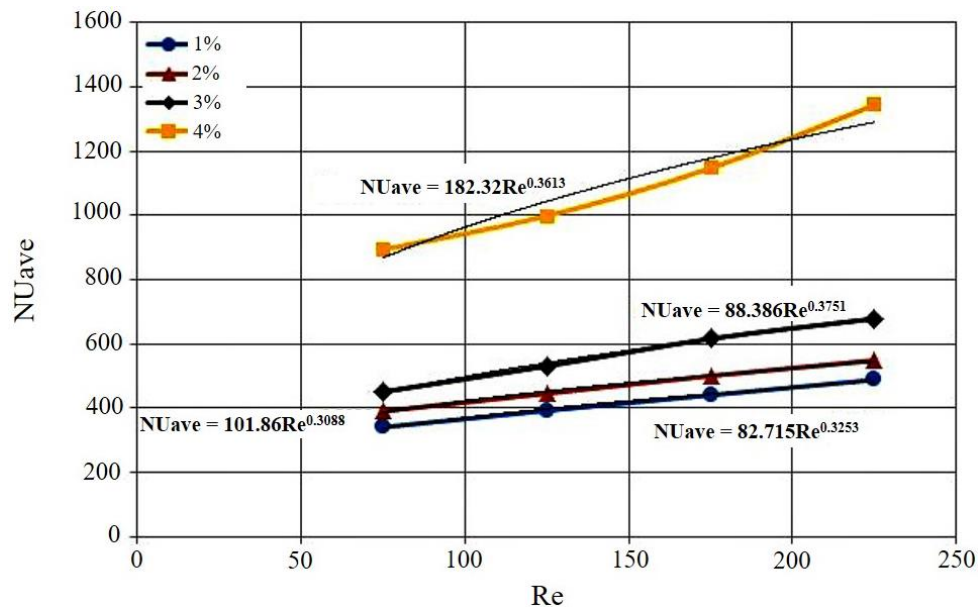
Figure 9 Average Nusselt number as a function of Reynolds number for different volume fractionvalues

Table 2 Average Nusselt number and pressure drop for different step height values

Non-dimensional step height	s/H = 0.5	s/H = 1	s/H = 1.5	s/H = 2
Nusselt number	799.63	548.20	487.71	428.98
Pressure drop	26.88	13.47	8.98	7.20

However, after the recirculation region, the decrease in the Nusselt number is more for higher step height values. In fact, as a result of the stronger mixing of the flow, the thermal boundary layer grows faster after the reattachment point.

The average Nusselt number has been presented in Table 2. It can be concluded increasing the step height decreases the average Nusselt number.

Based on the results presented in Figure 9 and Table 2 the pressure drop decreases with the step height. In other words, when the expansion ratio increases less pressure drop is experienced.

4.4. Volume fraction effect

In this section, the volume fraction effect is studied on the Nusselt number and pressure drop. The Reynolds number

and nanoparticles diameter are 225 and 10 nm, respectively. Figure 13 shows the variations of the Nusselt number along the channel for different volume fraction values. The Nusselt number increases with the nanoparticle's volume fraction. The reason is that the nanofluid has better thermal properties than the base fluid. The increase in the Nusselt number is considerable for volume fraction of 0.04. Figure 14 shows the variations of the pressure along the channel for various volume fraction values. The values of the average Nusselt number and pressure drop versus volume fraction have been presented in Table 3. The pressure drop increases by increasing the volume fraction. Note that when the volume fraction is 0.04, the pressure drop increases drastically. However, the increase in the Nusselt number is more considerable in this case. It should be noted that the use of higher volume fraction values is not necessarily useful. The

Table 3 Average Nusselt number and pressure drop for different volume fraction values

Volume fraction	1%	2%	3%	4%
Nusselt number	487.94	548.20	678.10	1344.03
Pressure drop	6.79	13.47	42.74	1457.71
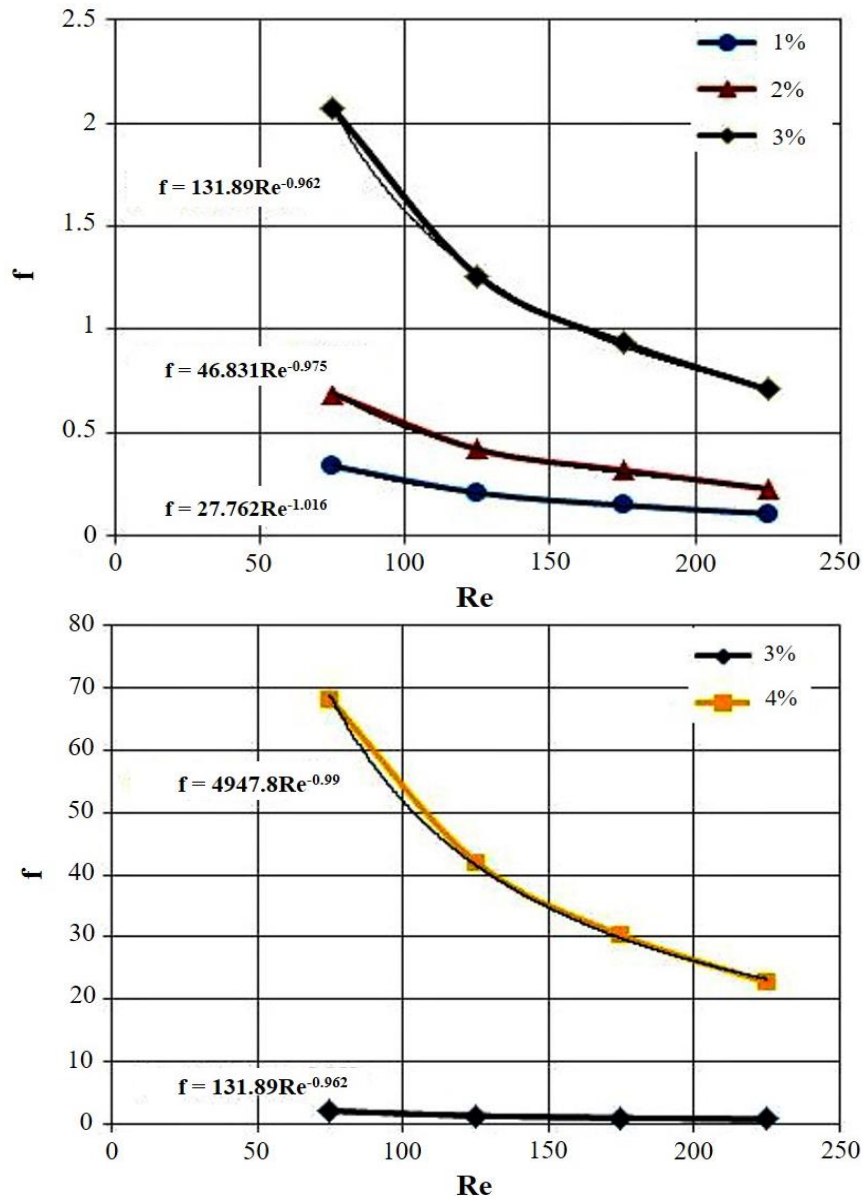
Figure 10 Average friction factor as a function of Reynolds number for different volume fractionvalues

reason is the intense pressure drop of the flow at higher nanoparticle concentrations.

4.5. Nanoparticle's diameter effect

In this section, the nanoparticle's diameter effect on the Nusselt number and pressure drop is considered. The Reynolds number and volume fraction are 225 and 0.02, respectively. Figures 15 and 16 represent the variations of the Nusselt number and pressure along the channel for different values of nanoparticle diameter. Also, the values of the pressure drop and average Nusselt numbers have been presented in Table 4. It is observed that the Nusselt number decreases with the nanoparticle diameter. However, this reduction is not severe. When the nanoparticle size increases

the Brownian part of the thermal conductivity decreases (equation (11)). On the other hand, the enhancement of the nanoparticle size leads to the reduction of the viscosity coefficient (equation (6)). The reduction of the viscosity and thermal conductivity is in a way that ultimately leads to the reduction of the Prandtl and subsequently Nusselt number. The pressure drop decreases with the nanoparticle diameter. The reason is the viscosity reduction as the nanoparticle size increases.

4.6. Nanoparticle type effect

In this section, the nanoparticle type effect on the pressure drop and Nusselt number is considered. The Reynolds number, volume fraction and nanoparticle

Table 4 The influence of the nanoparticles diameter on the average Nusselt number and pressure

Nanoparticle diameter	10 nm	20 nm	30 nm	40 nm
Nusselt number	548.20	520.86	509.21	502.44
Pressure drop	13.47	9.96	8.69	8.02
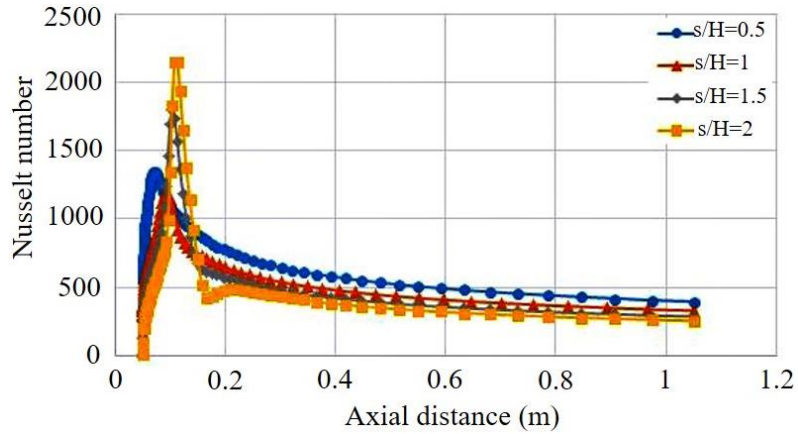
Figure 11 Variations of Nusselt number along the channel for different step height values
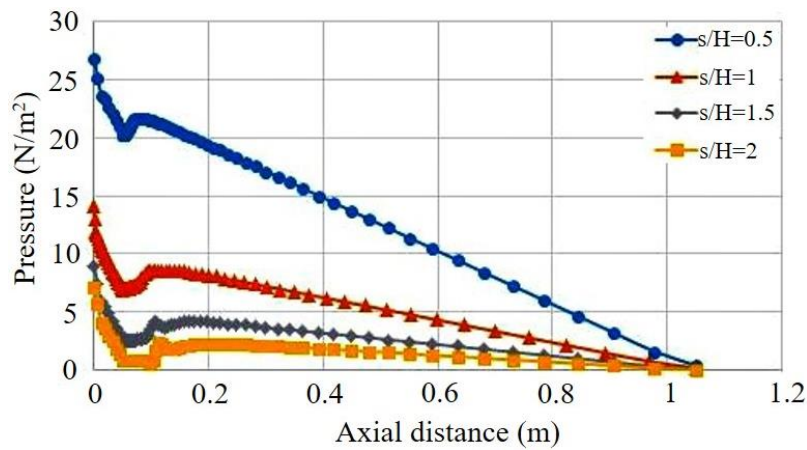
Figure 12 Variations of pressure along the channel for different step height values
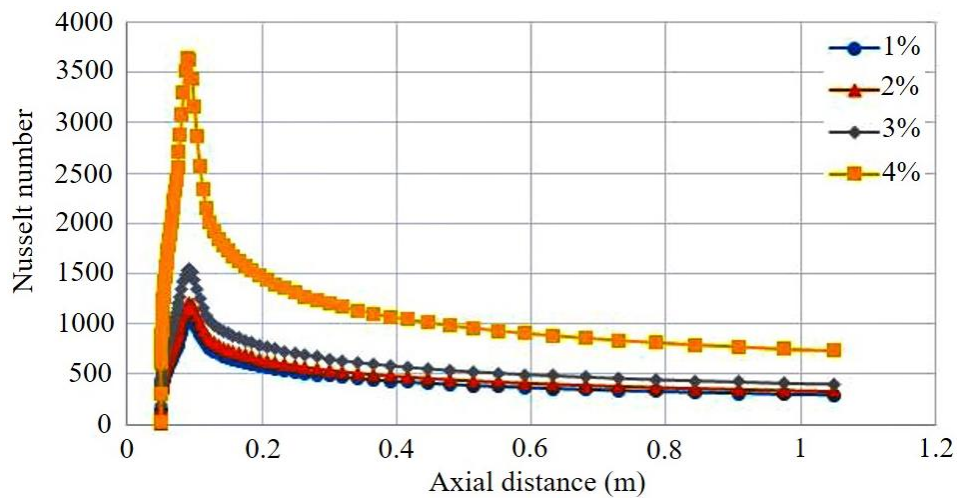
Figure 13 Variations of Nusselt number along the channel for different volume fraction values
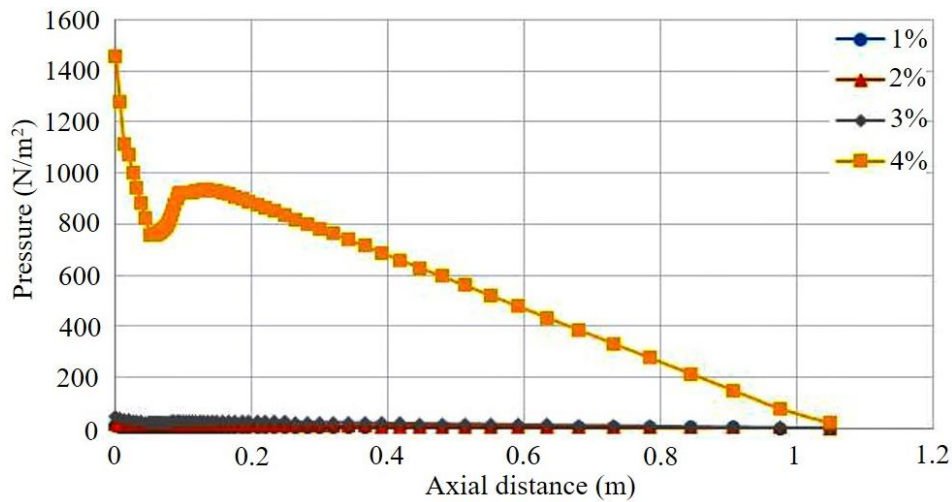
Figure 14 Variations of pressure along the channel for different volume fraction values
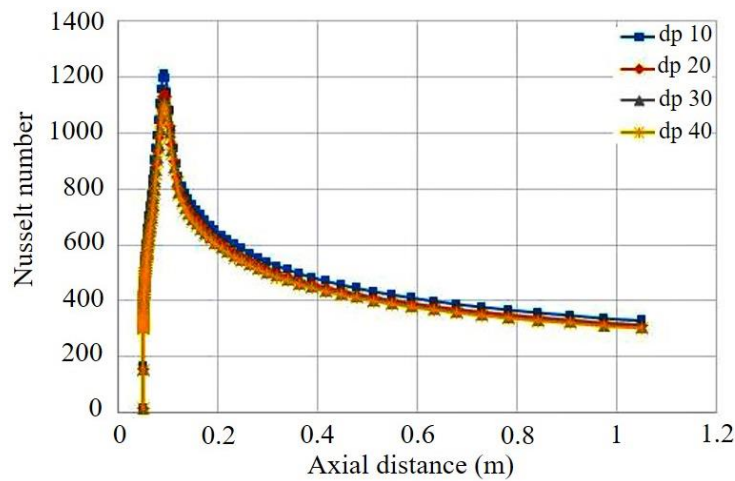
Figure 15 Variations of Nusselt number along the channel for different diameters of nanoparticles
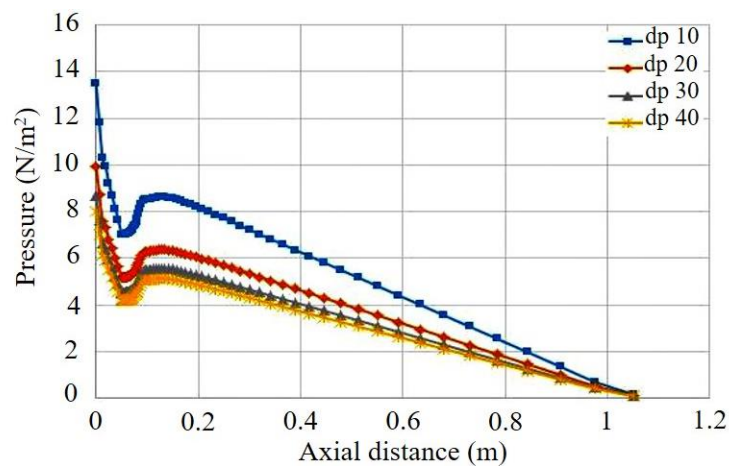
Figure 16 Variations of pressure along the channel for different diameters of nanoparticles

diameter are 225, 0.02 and 10 nm, respectively. Six nanoparticles were employed in this section. Figures 17 and 18 show the variations of the Nusslet number and pressure drop along the channel for different nanofluids. Also, the values of the pressure drop and average Nusselt number have been reported in Table 5. The maximum

and minimum average Nusselt numbers are related to TiO_2 and Al_2O_3 nanoparticles, respectively. However, the difference between the average Nusselt numbers of various nanoparticles is small. Also, there is not an important difference in the pressure drop of various nanoparticles.
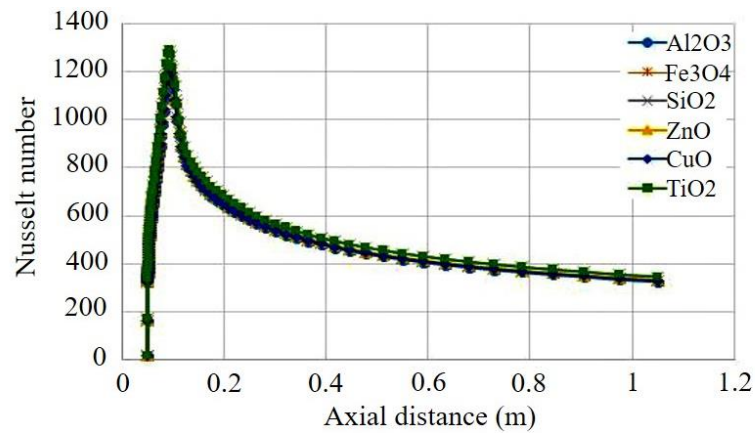
Figure 17 Variations of Nusselt number along the channel for different nanoparticles
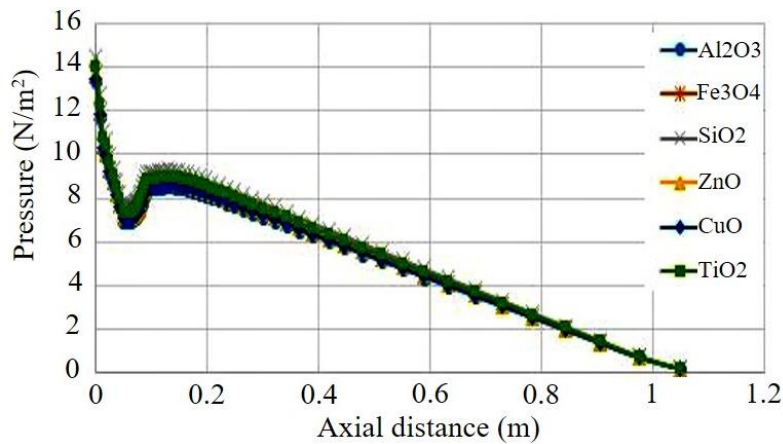
Figure 18 Variations of pressure along the channel for different nanoparticles

Table 5 The effect of the nanoparticle type on the average Nusselt number and pressure drop

Nanoparticle	Al₂O₃	Fe₃O₄	SiO₂	ZnO	CuO	TiO₂
Nusselt number	542.31	550.09	577.67	554.30	548.20	579.66
Pressure drop	13.37	13.64	14.48	13.69	13.47	14.05

4.7. Performance index

In this section, the performance of the system is evaluated for different Reynolds numbers and volume fraction values. For an accurate evaluation of the performance, the enhancement of both heat transfer coefficient and pressure drop in comparison with the pure fluid must be taken into account. For this purpose, the following performance index is defined [24-25]:

$$PI = \frac{\left(\frac{h_{nf}}{h_f}\right)}{\left(\frac{\Delta p_{nf}}{\Delta p_f}\right)} \tag{14}$$

In nanofluid systems, a performance index greater than 1 is desired. In this case, the enhancement of the heat transfer rate is higher than the enhancement of the pumping power. Figure 19 shows the performance index for various Reynolds numbers and volume fraction values. Based on this figure, the change of the Reynolds number in the studied range leads to a slight reduction in the performance index. For volume fraction values of 1% and 2%, the performance index is

greater than 1, whereas for volume fractions of 3% and 4% the performance index is less than 1. The reduction of the performance index for the volume fraction of 4% is very intense. In this case, the pressure drop increases drastically. This can be observed in Figure 14 for the Reynolds number of 225.

5. Conclusion

In this study, the flow and heat transfer of a nanofluid in a channel with a backward- facing step was studied by adopting the finite volume technique. The single-phase model was employed for modeling the effect of nanoparticles. The simulation results were validated against available data. The influence of various parameters on the pressure drop and Nusselt number were considered. The obtained results can be summarized as:

1. The presence of the step increases the local Nusselt number after the step due to the recirculation of flow. Nevertheless, increasing the step height decreases the average Nusselt number. Also, the pressure drop decreases with step height.
2. The pressure drop and Nusselt number increase by increasing the Reynolds number.
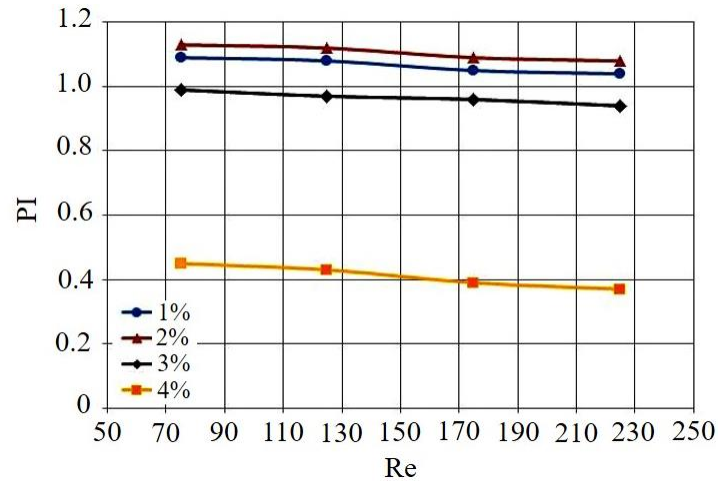
Figure 19 Variations of the performance index with Reynolds number and volume fraction

3. Increasing the nanoparticle's volume fraction increases both the pressure drop and Nusselt number. When the volume fraction increases to 0.04, a considerable enhancement of the Nusselt number is achieved. However, in this case, the pressure drop increases drastically.

4. The pressure drop and Nusselt number decrease with nanoparticle diameter.

5. Six types of nanoparticles (TiO$_2$, Fe$_3$O$_4$, CuO, Al$_2$O$_3$, ZnO, SiO$_2$) were compared. The maximum average Nusselt number was related to TiO$_2$ nanoparticles. The effect of the nanofluid type on the pressure drop was not considerable.

6. The performance index decreases with the Reynolds number slightly. The use of nanofluid with the concentrations of 3% and 4% is not appropriate. In these cases, the enhancement of the pumping power is more than the enhancement of the heat transfer rate.

6. References

[1] Addad Y, Laurence D, Talotte C, Jacob M. Large eddy simulation of a forward-backward facing step for acoustic source identification. Int J Heat Fluid Flow. 2003;24(4):562-71.

[2] Abu-Mulaweh H. Turbulent mixed convection flow over a forward-facing step—the effect of step heights. Int J Therm Sci. 2005;44(2):155-62.

[3] Chen Y, Nie J, Armaly B, Hsieh HT. Turbulent separated convection flow adjacent to backward-facing step—effects of step height. Int J Heat Mass Tran. 2006;49(19-20):3670-80.

[4] Abu-Nada E. Entropy generation due to heat and fluid flow in backward facing step flow with various expansion ratios. Int J Exergy. 2006;3(4):419-35.

[5] Lima R, Andrade C, Zaparoli E. Numerical study of three recirculation zones in the unilateral sudden expansion flow. Int Comm Heat Mass Tran. 2008;35(9):1053-60.

[6] Sherry M, Jacono DL, Sheridan J. An experimental investigation of the recirculation zone formed downstream of a forward facing step. J Wind Eng Ind Aerod. 2010;98(12):888-94.

[7] Bao F-b, Lin J-z. Continuum simulation of the microscale backward-facing step flow in a transition regime. Numer Heat Tran A: Appl. 2011;59(8):616-32.

[8] Kumar A, Dhiman AK. Effect of a circular cylinder on separated forced convection at a backward-facing step. Int J Therm Sci. 2012;52:176-85.

[9] Selimefendigil F, Öztop HF. Effect of a rotating cylinder in forced convection of ferrofluid over a backward facing step. Int J Heat Mass Tran. 2014;71:142-8.

[10] Togun H, Abdulrazzaq T, Kazi S, Badarudin A, Ariffin M, Zubir M. Numerical study of heat transfer and laminar flow over a backward facing step with and without obstacle. Int J Aero Mech Eng. 2014;8(2): 363-7.

[11] Niemann M, Fröhlich J. Buoyancy-affected backward-facing step flow with heat transfer at low Prandtl number. Int J Heat Mass Tran. 2016;101:1237-50.

[12] Xu J, Zou S, Inaoka K, Xi G. Effect of Reynolds number on flow and heat transfer in incompressible forced convection over a 3D backward-facing step. Int J Refrig. 2017;79:164-75.

[13] Juste G, Fajardo P. Influence of flow tree-dimensionality on the heat transfer of a narrow channel backward facing step flows. Int J Therm Sci. 2018;132:234-48.

[14] Al-Aswadi A, Mohammed H, Shuaib N, Campo A. Laminar forced convection flow over a backward facing step using nanofluids. Int Comm Heat Mass Tran. 2010;37(8):950-7.

[15] Kherbeet AS, Mohammed H, Salman B. The effect of nanofluids flow on mixed convection heat transfer over microscale backward-facing step. Int J Heat Mass Tran. 2012;55(21-22):5870-81.

[16] Selimefendigil F, Öztop HF. Identification of forced convection in pulsating flow at a backward facing step with a stationary cylinder subjected to nanofluid. Int Comm Heat Mass Tran. 2013;45:111-21.

[17] Kherbeet AS, Mohammed H, Munisamy K, Saidur R, Salman B, Mahbubul I. Experimental and numerical study of nanofluid flow and heat transfer over microscale forward-facing step. Int Comm Heat Mass Tran. 2014;57:319-29.

[18] Selimefendigil F, Öztop HF. Numerical study of forced convection of nanofluid flow over a backward facing step with a corrugated bottom wall in the presence of different shaped obstacles. Heat Tran Eng. 2016;37(15):1280-92.

[19] Selimefendigil F, Öztop HF. Forced convection and thermal predictions of pulsating nanofluid flow over a

backward facing step with a corrugated bottom wall. Int J Heat Mass Tran. 2017;110:231-47.

[20] Bouazizi L. Heat transfer enhancement in a backward-facing step with heated obstacle using nanofluid. Int J Automot Mech Eng. 2018;15(2):5195-210.

[21] Ekiciler R, Aydeniz E, Arslan K. A CFD Investigation of Al2O3/water flow in a duct having backward-facing step. J Therm Eng. 2019;5(1):31-41.

[22] Mohammed HA, Fathinia F, Vuthaluru HB, Liu S. CFD based investigations on the effects of blockage shapes on transient mixed convective nanofluid flow over a backward facing step. Powder Tech. 2019;346:441-51.

[23] Togun H, Safaei MR, Sadri R, Kazi SN, Badarudin A, Hooman K, et al. Numerical simulation of laminar to turbulent nanofluid flow and heat transfer over a backward-facing step. Appl Math Comput. 2014;239:153-70.

[24] Razi P, Akhavan-Behabadi MA, Saeedinia M. Pressure drop and thermal characteristics of CuO-base oil nanofluid laminar flow in flattened tubes under constant heat flux. Int Comm Heat Mass Tran. 2011;38:964-71.

[25] Zeinali Heris S, Ahmadi F, Mahian O. Pressure drop and performance characteristics of water-based Al_2O_3 and CuO nanofluids in a triangular duct. J Dispers Sci Technol. 2013;34:1368-75.